Available online at www.sciencedirect.com

ScienceDirect

Procedia Structural Integrity 2 (2016) 3697–3704

Structural Integrity Procedia

www.elsevier.com/locate/procedia

21st European Conference on Fracture, ECF21, 20-24 June 2016, Catania, Italy

Crack surface morphology and grain misorientation in fatigued aluminium alloy AA7050 samples after interrupted ageing and retrogression-reageing treatments

André L. M. Carvalho[a]*, Juliana P. Martins[b], Enrico Salvati[c], Tan Sui[c], Alexander M. Korsunsky[c]

[a]*Department of Material Engineering, State University of Ponta Grossa, 4748 General Carlos Cavalcanti Ave, Ponta Grossa 84030-900, Brazil*
[b]*Department of Chemical Engineering, Federal University of Technology–Paraná, Monteiro Lobato Ave, Ponta Grossa 84016-210, Brazil*
[c]*Multi-Beam Laboratory for Engineering Microscopy (MBLEM), Department of Engineering Science, University of Oxford, Parks Road, Oxford OX1 3PJ, United Kingdom*

Abstract

We present the investigation of fatigue crack surface morphology and crystallographic grain orientation in samples of aluminium alloy AA7050 that had been subjected to interrupted ageing (T6I4-65) and retrogression-reageing (RRA) heat treatments. Both T6I4-65 and RRA ageing treatments generate bimodal (particle size) microstructural features. A single tensile overload was applied and its influence on the crystallographic grain orientation was evaluated using electron backscatter diffraction (EBSD). The results reveal that T6I4-65 and RRA heat treatments contribute to the increased occurrence of planar slip features in the form of small and large flat facets, respectively. T6I4-65 condition leads to a greater degree of lattice misorientation in the vicinity of fatigue crack tip than the RRA condition which is likely to be the evidence of increased plastic deformation due to the overload.

Peer-review under responsibility of the Scientific Committee of ECF21.

Keywords: Fatigue fracture surface; EBSD; Misorientation; T6I4-65 and RRA conditions.

* Corresponding author. Tel.: +55- 42-3220-3340; fax: +55- 42-3220-3072.
E-mail address: andrelmc@uepg.br

Peer review under responsibility of the Scientific Committee of ECF21.
10.1016/j.prostr.2016.06.459

1. Introduction

AA7050-T7451 aluminium alloy finds widespread use in the manufacturing of aircraft structural components such as wing skins, fuselage frames and bulkheads. Its choice is attributed to the combination of high strength, fracture toughness, fatigue initiation and propagation resistance with the required stress corrosion cracking resistance. Typically, the overageing heat treatment T7451 has been applied to reduce the susceptibility of alloy to stress corrosion cracking. However, this heat treatment leads to a sacrificial reduction of the maximum strength of this alloy. Currently, multiple-stage ageing treatments are being developed for aluminium alloys to enhance their mechanical properties, e.g. Feng et al (2013). One suggestion has been to replace the traditional overageing heat treatment of this alloy with a three-step heat treatment called retrogression and re-ageing (RRA) treatment, e.g. Wang et al. (2014). Another new heat treatment designated T6I4 (I=interrupted) has also been applied to AA7050 aluminium alloy in order to overcome the inverse correlation between important tensile properties, such as yield strength and ductility, e.g. Burba et al. (2013). These properties are directly related to the interaction between the mobile dislocations and obstacles to their movement from bimodal microstructure containing both shearable and shear-resistant precipitates generated by multiple-stage ageing schedules, e.g. Chen et al. (2013). Microstructural effects are known to have a strong influence on fatigue crack growth rates via the activation of competing mechanisms operating during fatigue crack propagation.

A large number of studies have been performed to determine the relationship between microstructure and mechanical properties. Electron Back Scatter Diffraction (EBSD) has gained popularity due to its ability to reveal spatially resolved information about the crystallographic orientation and misorientation within alloy grains, and allowing to relate the spatial distribution of plastic deformation with microstructural characteristics, as described by Haskel et al. (2014). EBSD technique permits the study of the effects of fatigue-induced crystal defects on the crack path and the pre-existing defect structure, i.e. grain/subgrain boundaries, as shown by Gupta et al. (2012). However, few studies have explored the potential of multi-stage ageing treatments on the fatigue crack propagation paths using EBSD technique.

The purpose of this study was to elucidate the role of the microstructure, including grain and subgrain boundaries, and crystallographic (mis)orientation on the fatigue crack propagation path in samples made from Al alloy plates processed using the (T6I4-65) interrupted ageing and (RRA) retrogression ageing treatments. Both ageing heat treatments produce bimodal microstructure containing shearable and shear-resistant precipitates, the difference between their response arises due to the specific competition between physical deformation mechanisms. A single overload was applied to a sample containing steadily grown fatigue to assess its influence on the crystallographic orientation through the use of EBSD analysis.

2. Experimental procedure

AA7050-T7451 aluminium alloy plate of 76.8mm thickness used in this study had the composition (in wt%) of 5.58Zn, 1.88Mg, 2.00Cu, 0.07Fe, 0.02Si, 0.15Zr, Al balance and was provided by the Embraer Company. Specimens were removed from the rolling direction (RD). The tensile properties of the material in the T6I4-65 and RRA conditions were: the ultimate tensile strength (UTS) of 534 MPa and 613.20 MPa, the yield strength of 452 MPa and 540 MPa, and the reduction in area of 38.2 % and 22.8%, respectively.

2.1. Heat treatment

In the present study two types of ageing heat treatment were used. The first was a two stage treatment designated the T6I4-65 condition, which involved solution treatment at 485 °C for 4 h, quenched into cold water, aged at 130 °C for 15 min, quenched again and aged at 65ºC for two months. The second heat treatment was three stage and designated as the RRA condition; alloy was solution treated at 485 °C for 4 h, water quenched, and aged at 130°C for 24h followed by retrogression at 185°C for 20 min, followed by ageing at 65ºC for two months.

2.2. Fatigue testing

Fatigue crack propagation testing was carried out under constant stress amplitude using a servohydraulic 15 kN fatigue rig. Compact tension (CT) specimens were machined from the plate with T-L orientation of width 28 mm and thickness 2.8 mm. All samples were pre-cracked as described in ASTM E 647 (2005). Crack length was measured using the digital camera attached to a Questar long-range telescope. Fatigue testing took place with maximum load of 1.3 kN using a frequency of 10 Hz and the stress ratio R of 0.3.

Moreover, a single overload (OL) of 100% was applied, and its influence was investigated on the fatigue fracture surface and local grain (mis)orientation for the samples in T6I4-65 and RRA conditions. The overload force of 2.6 kN was applied when the crack length reached ~3.0 mm. The samples in the two conditions were then loaded further under the previously applied cyclic fatigue conditions to 1.73×10^5 cycles and 1.42×10^5 cycles, respectively. Following the experiments, the morphology of crack propagation was studied at locations corresponding to before and after the overload region. This was observed by electron backscattered diffraction technique implemented in the scanning electron microscope (SEM-EBSD).

2.3. Fracture surface analysis

Fracture surface analysis was performed at the regions of crack growth in the low and high ΔK regimes, for both the T6I4-65 and RRA conditions. All fracture analysis and imaging were carried out using Tescan FIB-SEM LYRA-3XM with the secondary electron imaging mode.

2.4. EBSD analysis

The samples were ground using 600-4000 grit SiC papers followed by polishing with 3 and 1 μm water-based diamond slurry. Finally, polishing in the solution of OP-S (colloidal silica) was performed.

Crystallographic orientations from fatigue crack propagation length were obtained using EBSD on a Tescan FIB-SEM equipped with a NordlysNano NL-04 high speed CCD camera and HKL technology Channel 5.0 software from Oxford Instruments.

Accordingly, the orientation and misorientation maps were obtained on the TD-RD plane which the fatigue crack propagated (Fig. 2a-b) using step size 0.26 - 1.85 μm and magnification of 800-1950 times for both T6I4-65 and RRA conditions.

3. Results and discussion

3.1. Fracture surface analysis

Fig. 1a-b shows the results of fractographic analysis performed by SEM at the fracture surfaces in the low ΔK regime for the T6I4-65 and RRA conditions. In the present work, the RRA condition exhibited a predominance of large flat fracture facets at low to moderate ΔK level, whilst the T6I4-65 condition revealed a prevalence of small flat facets. For both conditions shallow pockets were also observed. These features for the T6I4-65 condition can be seen in Fig 1a which shows flat facets (black arrows) containing multiple wavy regions highlighting the influence of the underlying grain structure. It is concluded that both ageing conditions contributed to the increased occurrence of planar slips with large and small flat facets, as a consequence of the competing deformation mechanisms engendered by the bimodal microstructure.

In the AA7050 alloy the slip is classified into two categories. Firstly, the wavy slip bands reveal a homogeneous structure. Secondly, planar slip bands indicate that a heterogeneous structure predominates, according to De et al (2011). The second phenomenon is known as slip planarity due to it being the main driving force in fatigue crack propagation. This evidence can be seen Fig. 1b that shows fractography of the RRA condition, indicating that the crack propagation direction shows a significant deflection at the twist grain boundary. The same feature was found by Jian et al. (2010) in the T7451 Al-Zn-Mg-Cu alloy.

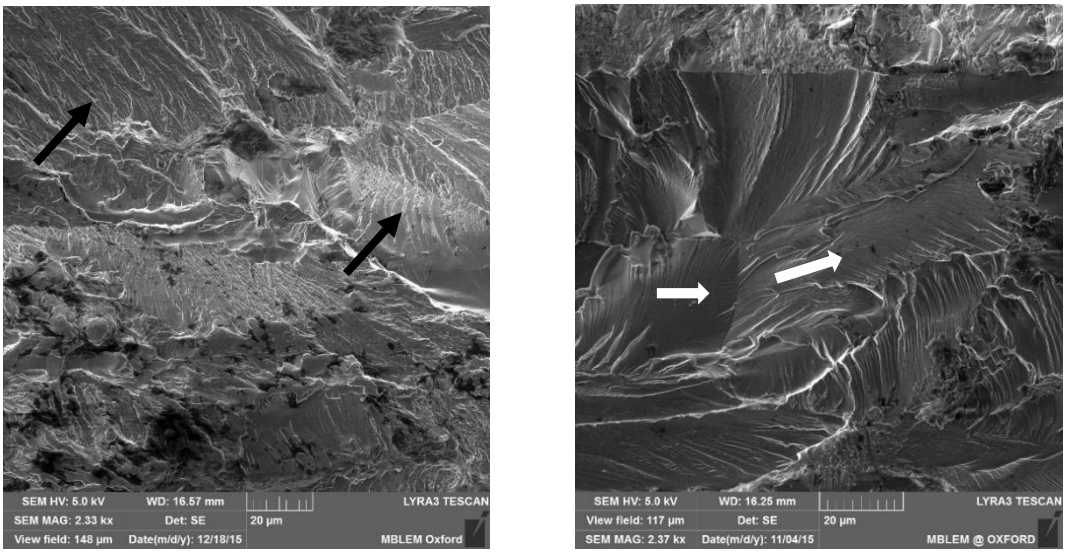

Fig. 1. SEM fractographs of the fracture surface of the alloy in the two conditions (a) T6I4-65 black arrow shows flat facets containing multiple wavy regions and (b) RRA white arrows highlight the crack growth patterns change in the propagation direction of crack at the twist grain boundary (crack propagation direction is from left to right).

3.2. EBSD analysis

In the present study EBSD analysis was performed on small regions of ~750µm along the crack located in the vicinity of the overload location, as well as before and after it for both the T6I4-65 and RRA conditions. For both conditions the EBSD orientation maps revealed two types of microstructure, that is, recrystallized grains that showed relative lack of substructure, while others grains were not recrystallized and contained clear subgrain structure.

SEM images in Figs. 2a-b display the crack path in the TD-RD plane with the respective regions that were investigated for the T6I4-65 and RRA conditions. In these images it is possible to notice some features such as the occurrence of crack orientation changes (deflection) along crack length before and after overload regions (encircled 1 and 2), as also, the closed region of crack after overload regions for both conditions.

Figs. 2c-d shows the EBSD orientation maps (IPF maps) obtained from the microstructures of regions I and II for the T6I4-65 and RRA conditions, respectively. Moreover, in the inverse pole-figure maps (Figs. 2c-d) were also superposed, and low and high angle grain boundaries indicated. It was used black thin lines to identify low angle boundaries ($1° \leq \theta \leq 15°$) and black thick lines to characterize high angle boundaries ($\theta > 15°$). It is possible to notice the presence of unrecrystallized grains which contains high density of low angle boundaries into grains. And also grains recrystallized which are described as absence low angle boundaries into grains. Besides, it can be deduced from the high density of low-angle boundaries confined very near the fatigue crack wake, mainly at the overload regions (black arrows), that a region of high plastic deformation lies adjacent to the crack propagation path for both T6I4-65 and RRA conditions. For both conditions the EBSD orientation maps (Figs 2c-d) show that the crack propagation path was predominantly transgranular, however, intergranular crack propagation was also observed.

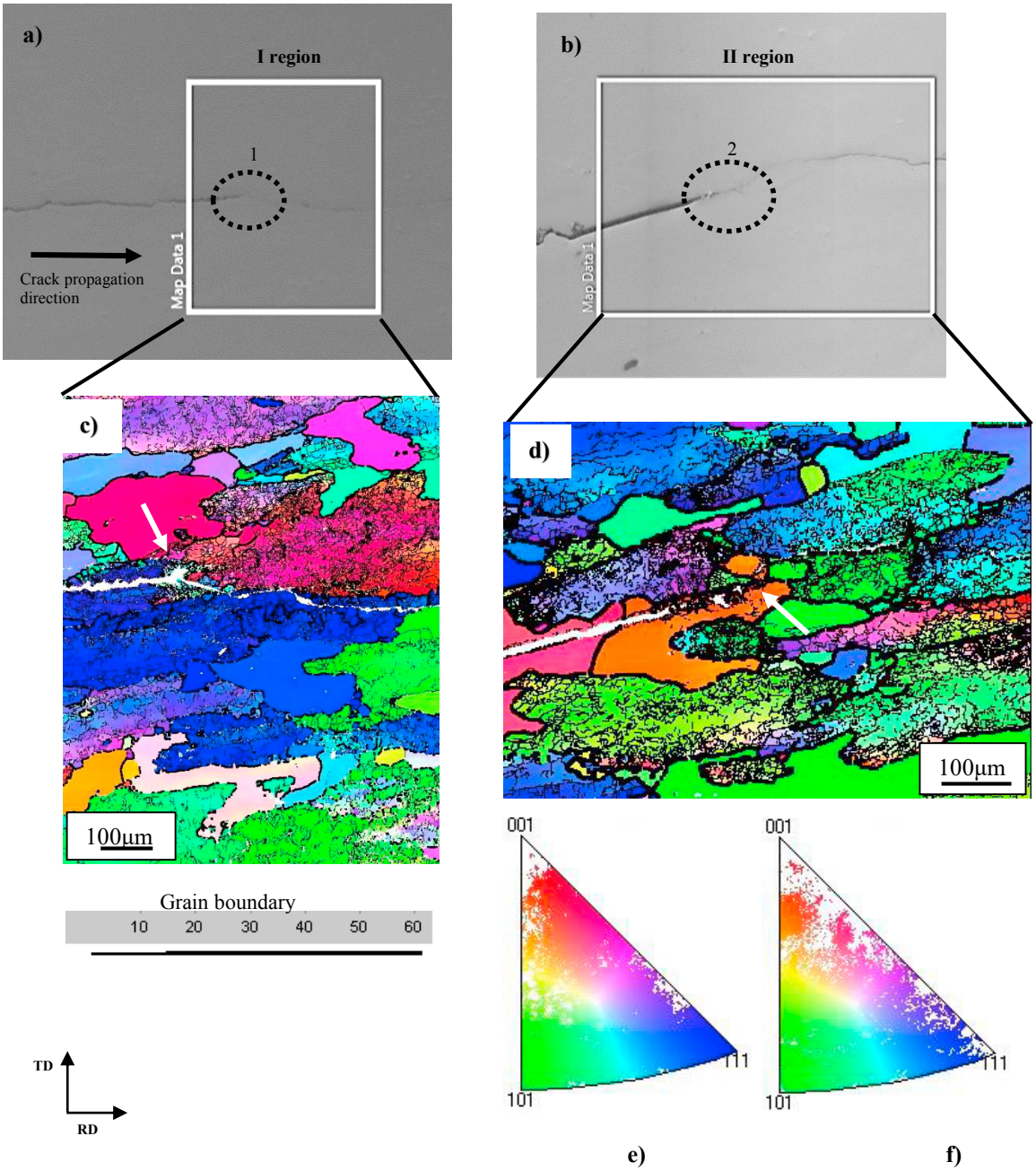

Fig. 2. (a) and (b) SEM micrographs show the plane which the fatigue crack propagated (RD) obtained from the T6I4-65 and RRA conditions, respectively. Encircled regions (1 and 2) in the SEM images illustrate the regions which overload occurred, notice also crack deflection for both conditions. (c) and (d) orientation distribution maps from the I and II regions, respectively. (e) and (f) EBSD inverse pole-figures (IPF X) of both I and II regions, respectively.

The inverse pole figures (IPF) in Figs.2e-f reveal a large orientation spread for both the T6I4-65 and RRA conditions. This phenomenon can be associated with partial recrystallization that occurs during the heat treatment. A study performed by Robson and Prangnell (2002) on the AA7050 T7451 aluminium alloy reported that partial recrystallization takes place in the neighbourhood of intermetallic particles during solution heat treatment. In the present work, the 7050 alloy underwent two stage of solution heat treatment for both conditions.

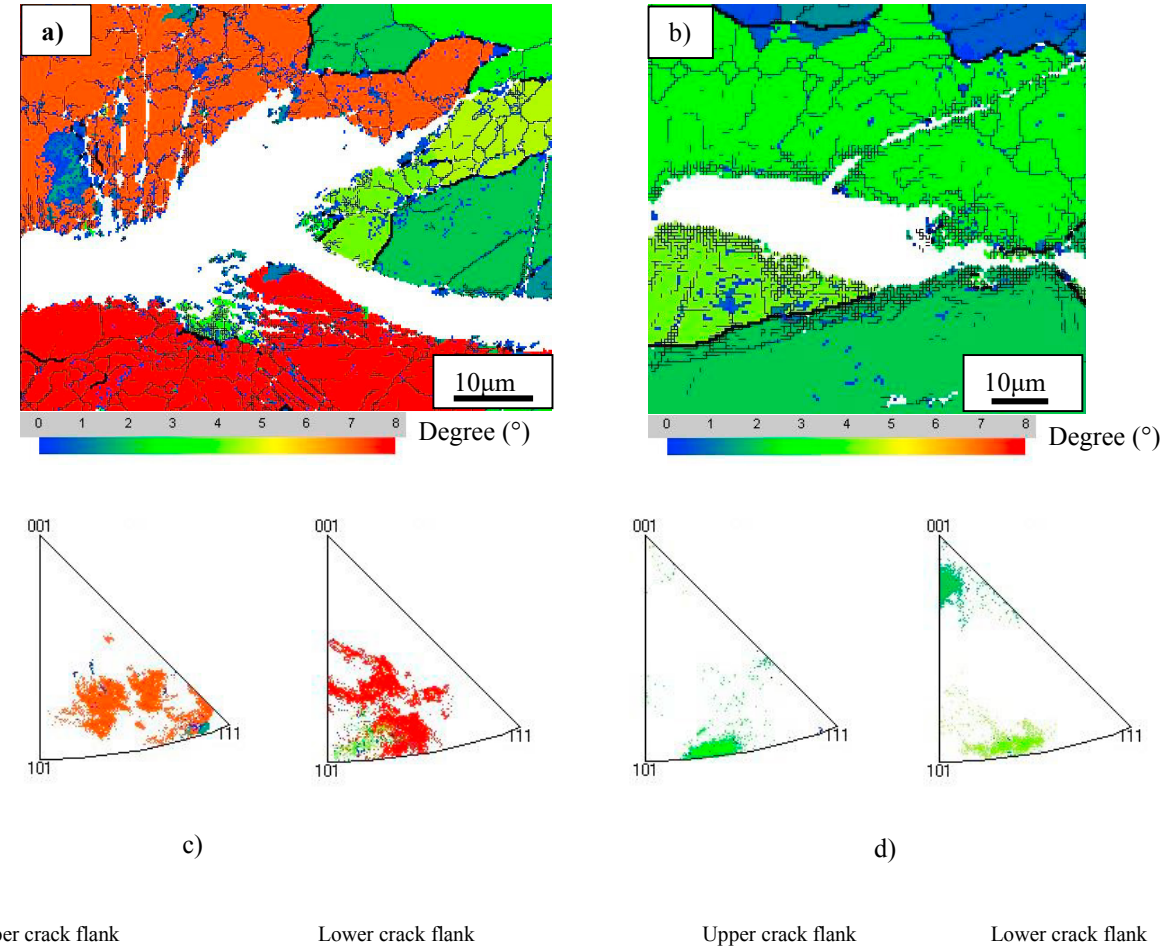

Fig. 3. Plastic deformation zone regions as consequence of applied overload is shown at the crack flank corresponding the encircled (1 and 2 of Figs. 2a-b) regions. (a) and (b) mean misorientation maps from the T6I4-65 and RRA conditions; respectively. (c) IPF triangle projections for the upper and lower sides of the crack wake from the T6I4-65 condition; (d) IPF triangle projections for the upper and lower sides of the crack wake from the RRA condition.

In order to understand better the influence of applied overload on the two conditions, the investigation of the average misorientation maps (mean misorientation) was performed locally to the regions where the overload occurred. The mean misorientation was determined by the average of subgrain orientation within each grain from three Euler angles (φ_1, Φ, φ_2). The average misorientation was set to the lattice or pixel orientation of EBSD, following the technique by Gupta et al. (2010).

The average misorientation maps can be seen in Figs. 3a-b, which display the difference of misoriented area (indicated by difference in colors in the maps) at the overload regions and the crack wake. It is concluded that these different misoriented areas correspond to the plastic deformation zone associated with applied overload at the crack

wake for both conditions. Thus, the misoriented area with 8° (red color in Fig 3a) indicates higher density of subgrain structure (low-angle boundary) than the misoriented area with 4° (light green color in Fig. 3b) for both T6I4-65 and RRA conditions. In this case, it is revealed that a gradient of misorientation corresponds to the minimum to maximum misorientation angle between 0 - 8°. Hughes-Hansen (1997) reported that the tendency of grain towards subdivision is distinctly orientation-dependent. The deformation behavior of each grain depends clearly on its initial orientation. It is known that for some orientations deformation takes place in a stable manner producing low misorientation, according to Sandim et al. (2001). These observations can explain the regions with low misorientation (blue color on the scale) even in the plastic deformation zone due to the applied overload, as shown in Figs. 3c-d.

Moreover, the orientation with respect to the laboratory coordinate system was determined and is presented using IPF triangle projections for the upper and lower shores of the crack in the overload region for both T6I4-65 and RRA conditions, as can be seen in Figs3 c-d. For the T6I4-65 condition (Fig. 3c) it is noted that the orientation is equally spread for both sides of the crack wake. In contrast, for the RRA condition a clear difference is observed between the lower and upper flanks of the crack wake, as can be seen in Fig. 3d.

It was recently reported by Chen et al. (2013) that multistage ageing treatment produce bimodal microstructures containing both shearable and shear resistant precipitates that contribute to the increase in the occurrence of planar slips. In the AA7050 aluminium alloy these planar slips display wavy slip features, as described by De et al. (2011). However, it is surmised that these features of the planar slips shown in Figs 1a-b can contribute to the formation of substructure with different misoriented areas illustrated in Figs 3a-b.

4. Concluding remarks

The present study investigated the fractographic features as well as grain misorientation in fatigue samples from two types of ageing heat treatment, that is, interrupted ageing and retrogression-re-ageing conditions. Both T6I4-65 and RRA ageing treatments are known to generate bimodal microstructure features. A single tensile overload was applied and its influence evaluated on the crystallographic orientation using automated EBSD. The results obtained are summarized below.

Both conditions contribute to the increase in the occurrence of planar slips which feature large flat facets for the RRA condition and small flat facets for the TI4-65 conditions, as consequence of competing mechanisms from bimodal microstructure.

EBSD analysis has shown that both T6I4-65 and RRA conditions reveal transgranular and intergranular behaviour,, as well as crack deflection along the its path length.

T6I4-65 condition has shown higher misorientation density than the RRA condition, indicating higher plastic deformation zone as the consequence of the applied overload.

IPF triangle projection analysis for the T6I4-65 condition has shown that the population misorientation density was spread widely. This suggests that the applied overload contributed to the increase in the orientation anisotropy within the region.

Acknowledgements

This work was supported in part by the CAPES under Grant BEX 2606/15-1 and BEX 2638/15-0. AMK acknowledges funding received for the MBLEM laboratory at Oxford through EU FP7 project iSTRESS (604646) and access to the facilities at the Research Complex at Harwell (RCaH), under the Centre for In situ Processing Studies (CIPS).

References

ASTM Test Methods for Measurement of Fatigue Crack Growth Rates, 2005, ASTM Standard, E 647-95a.

De, P.S., Mishra, R.S., Baumann, J.A., 2011. Characterization of High Cycle Fatigue Behavior of a New Generation Aluminum Lithium Alloy. Acta Materialia 59, 5946–5960.

Jian, H., Jiang, F., Wei, L., Zheng, X., Wen, K., 2010. Crystallographic Mechanism for Crack Propagation in the T7451 Al–Zn–Mg–Cu Alloy. Materials Science and Engineering A 527, 5879–5882.

Robson, J.D., Prangnell P.B., 2002. Predicting Recrystallised Volume Fraction in Aluminium Alloy 7050 Hot Rolled Plate. Materials Science and Technology 18, 607-614.

Chen, Y., Weyland, M., Hutchinson, C.R., 2013. The Effect of Interrupted Aging on the Yield Strength and Uniform Elongation of Precipitation-Hardened Al Alloys. Acta Materialia 61, 5877–5894.

Sandim H.R.Z., Martins J.P., Padilha A. F., 2001. Orientation Effects During Grain Subdivision and Subsequent Annealing in Coarse Grained Tantalum. Scripta Materiallia 45, 733-738.

Haskel, H.L., Pauletti, E., Martins, J.P., Carvalho, A.L.M., 2014. Microstructure and Microtexture Assessment of Delamination Phenomena in Charpy Impact Tested Specimens. Materials Research 17, 1238-1250.

Hughes, D.A., Hansen, N., 1997. High Angle Boundaries Formed by grain subdivision mechanisms. Acta Materiallia 45, 3871-3886.

Gupta V. K., Agnew, S. R., 2010. A Simple Algorithm to Eliminate Ambiguities in EBSD Orientation Map Visualization and Analyses: Application to Fatigue Crack-Tips/Wakes in Aluminum Alloys. Microscopy and Microanalysis, 16, 831–841.

Gupta, V.K., Gangloff, R.P., Agnew, S.R., 2012. Diffraction Characterization of Microstructure Scale Fatigue Crack Growth in a Modern Al–Zn–Mg–Cu alloy. International Journal of Fatigue 42, 131–146.

Feng, D., Zhang, X.M., Liu, S.D., Wang, T., Wu, Z.Z., Guo, Y.W., 2013. The Effect of Pre-Ageing Temperature and Retrogression Heating Rate on the Microstructure and Properties of AA7055. Materials Science & Engineering A 588, 34–42.

Wang, Y.L., Pan, Q.L., Wei, L.L., Li, B., Wang, Y., 2014. Effect of Retrogression and Reaging Treatment on the Microstructure and Fatigue Crack Growth Behavior of 7050 Aluminum Alloy Thick Plate. Materials and Design 55, 857–863.